Quantum state tomography for quadrupolar nuclei using global rotations of the spin system

J. Teles[a] and E. R. deAzevedo[b]
Instituto de Física de São Carlos, Universidade de São Paulo, P.O. Box 369, São Carlos 13560-970, São Paulo, Brazil

R. Auccaise, R. S. Sarthour, and I. S. Oliveira
Centro Brasileiro de Pesquisas Físicas, Rua Dr. Xavier Sigaud 150, Rio de Janeiro 22290-180, Rio de Janeiro, Brazil

T. J. Bonagamba
Instituto de Física de São Carlos, Universidade de São Paulo, P.O. Box 369, São Carlos 13560-970, São Paulo, Brazil

(Received 12 January 2007; accepted 22 February 2007; published online 17 April 2007)

In this paper, we describe a quantum state tomography method based on global rotations of the spin system which, together with a coherence selection scheme, enables the complete density matrix reconstruction. The main advantage of this technique, in respect to previous proposals, is the use of much shorter rf pulses, which decreases significantly the time necessary for algorithm quantum state tomography. In this case, under adequate experimental conditions, the rf pulses correspond to simple spatial rotations of the spin states, and its analytical description is conveniently given in the irreducible tensor formalism. Simulated results show the feasibility of the method for a single spin 7/2 nucleus. As an experimental result, we exemplify the application of this method by tomographing the steps during the implementation of the Deutsch algorithm. The algorithm was implemented in a ^{23}Na quadrupole nucleus using the strongly modulated pulses technique. We also extended the tomography method for a 3-coupled homonuclear spin 1/2 system, where an additional evolution under the internal Hamiltonian is necessary for zero order coherences evaluation. © *2007 American Institute of Physics*. [DOI: 10.1063/1.2717179]

I. INTRODUCTION

The characterization of the state of a quantum system is one of the most important steps in quantum physics and, in particular, in quantum computing (QC).[1–5] In general, the readout operation after the execution of a quantum algorithm is encoded in one of the system eigenstates of the computational basis, but the execution of the individual quantum logical gate usually involves the creation of many quantum coherences that may play a crucial rule in the execution of the algorithm. Therefore, in many occasions it is necessary to know all the elements of the density matrices that characterize a quantum system, which is usually named as quantum state tomography (QST). Besides, mapping the density matrix of a quantum system provides a way of extracting the maximum information available and allows many interesting applications, such as (i) testing the preparation of quantum states, (ii) estimating the experimental errors and calculating the fidelity of a quantum gate, (iii) monitoring the implementation of quantum gates in intermediate steps, (iv) characterizing decoherence and dissipation effects in quantum systems, (v) calculating the quantum entropies of the individual qubits, (vi) monitoring the Bloch vector trajectories during a quantum logical operation, etc.

Nuclear magnetic resonance (NMR) has provided unique methods for demonstrating the realization of quantum logical operations and characterizing the quantum state of spin systems. The great success achieved so far by NMR quantum computing is related to its ability for controlling the dynamics of the spins through rf pulses. This capacity made possible to prepare adequate initial states, perform unitary transformations that implement logical gates, and fully characterize the resulting states, i.e., to execute all crucial steps for QC. The quick achievements reached by NMR are also directly related to the fact that NMR has a long tradition in characterizing and monitoring the evolution of spin systems, including methods for exciting and detecting multiple quantum coherences in solution and solid state samples.[6] Besides, many of the ideas introduced by NMR QC experiments can become useful, with little modifications, in other areas of QC. One of the major achievements of NMR QC was the possibility of characterizing the quantum state of the system through the quantum state tomography. The first NMR QST method was developed by Chuang *et al.*[7] and optimized by Long *et al.*[8] for systems of heteronuclear coupled spins 1/2. It consists basically in applying a set of specially designed rotations on the different spins and reconstructing the density matrix from the resulting NMR spectra. This method was later adapted for homonuclear coupled spins 1/2 (Ref. 9) and also for quadrupolar spin 3/2 systems,[10–13] where nonselective pulses were replaced by transition-selective rf pulses. The main disadvantages of us-

[a]Electronic mail: jteles@ifsc.usp.br
[b]Electronic mail: azevedo@ifsc.usp.br

ing selective pulses are that they can introduce significant errors in the rotations, and its duration is usually much longer than for nonselective pulses. Furthermore, the system is also evolving during the QST process. This not only decreases the time available for executing the logical operations, but also makes more difficult the experimental control of the pulses actions. A QST method that is particularly useful for large systems was also developed. It is based on the two-dimensional Fourier transform technique and has the advantage of not using selective pulses.[14] However, in this two-dimensional approach it is necessary to use extra evolution periods, and the duration of the QST pulse sequence is as long as for the methods that use selective pulses. This limitation can be particularly prominent for quadrupolar or strongly coupled spins systems.

The article reports a QST NMR method that is specially suitable for single quadrupolar nuclei. The method is based on the selection of coherences provided by hard rf pulses applied with appropriated choice of phases and amplitudes. In principle, the method can be adapted for any spins system, including coupled spins 1/2 and single or coupled quadrupolar spins systems. Besides, it is based on general rotation properties that can be easily adapted for application other than NMR.[15–17] However, the advantage of using only global rotations in the tomography processes is only obtained for single quadrupolar spin systems, as discussed in Sec. III B. First, in Sec. II, the general theory is developed on the framework of rotations of general spins systems using the irreducible spherical tensor representation. The application for single quadrupolar nuclei is given in Sec. III A, together with a simulation for the spin 7/2 case and the experimental implementation of the Deutsch algorithm, via strongly modulated pulses (SMP) technique[18] in the spin 3/2 ^{23}Na nucleus. In Sec. III B the method is discussed in the context of homonuclear coupled spins systems, and the tomography simulation for a three coupled spin 1/2 system is showed. Some discussions involving heteronuclear spins systems are made in Sec. III C. The experimental setup used in this work is given in Sec. IV and the conclusions are made in Sec. V.

II. METHOD DESCRIPTION

A. The effect of nonselective rf fields

Let us start by considering the nature of the Hamiltonians usually utilized in NMR QC. For molecules in liquids comprising systems of N coupled nuclei, the Hamiltonian normally simplifies to the following expression:

$$\mathcal{H} = -\hbar\sum_{i=1}^{N}\omega_0^i\mathcal{I}_z^i + 2\pi\hbar\sum_{i=1}^{N}\sum_{j<i}J_{ij}\mathcal{I}_z^i\mathcal{I}_z^j + \mathcal{H}_{\mathrm{rf}}, \tag{1}$$

where $\omega_0^i=(1-\sigma_i)\gamma_i B_0$ accounts for the Larmor frequency and chemical shift of each nucleus, and J_{ij} is the scalar coupling between nuclei pairs. Here, $\mathcal{H}_{\mathrm{rf}}$ is an external time-dependent perturbation that can be applied by means of a controllable rf pulse. The liquid state is preferable for QC mainly due to the simplicity of its Hamiltonian. However, in solid systems it is also possible to obtain a Hamiltonian similar to Eq. (1) by considering the direct magnetic dipolar coupling between the nuclei in place of the scalar coupling.

Usually, N nuclei with spin 1/2 are used to form a N-qubit system, though systems with only one nucleus with spin greater than 1/2 under the presence of an electric field gradient can also be used. In this case, the interaction between the nuclear electric quadrupole moment and the electric field gradient gives rise to the so-called electric quadrupole interaction, which is represented in first order by the following Hamiltonian:

$$\mathcal{H} = -\hbar\omega_0\mathcal{I}_z + \frac{\hbar\omega_q}{6}(3\mathcal{I}_z^2 - \mathcal{I}^2) + \mathcal{H}_{\mathrm{rf}}. \tag{2}$$

Therefore, a general form of the Hamiltonian can be written considering three contributions,

$$\mathcal{H} = \mathcal{H}_0 + \mathcal{H}_{\mathrm{int}} + \mathcal{H}_{\mathrm{rf}}. \tag{3}$$

where

$$\mathcal{H}_0 = -\hbar\sum_{i=1}^{N}\omega_0^i\mathcal{I}_z^i, \tag{4a}$$

$$\mathcal{H}_{\mathrm{int}} = \hbar\sum_{i=1}^{N}\sum_{j\leqslant i}\omega_{ij}\mathcal{H}_{ij}. \tag{4b}$$

The dimensionless $\mathcal{H}_{ij}$ contributions are responsible for any interaction between the spin pairs, and the constants ω_{ij} give the coupling strengths. The summation includes terms $i=j$ that may correspond to the quadrupolar contribution.

We will use the following rf field:

$$\mathbf{B}_1(t) = \sum_{r=1}^{N_S}B_1^r[\cos(\bar{\omega}_0^r t+\phi_r)\hat{x} + \sin(-\bar{\omega}_0^r t+\phi_r)\hat{y}]. \tag{5}$$

The frequencies $\bar{\omega}_0^r$ are defined as the average frequencies for each nuclear species r, i.e., $\bar{\omega}_0^r=(1/n_r)\Sigma_{i=1}^{n_r}\omega_0^{\{ri\}}$. To indicate the ith nucleus of the rth nuclear species we refer to the index $\{ri\}$. The index r runs from 1 to N_S while i runs from 1 to n_r, characterizing N_S nuclear species with n_r nuclei of each species. Thus, the rf Hamiltonian becomes

$$\mathcal{H}_{\mathrm{rf}}(t) = -\hbar\sum_{r=1}^{N_S}\sum_{i=1}^{N}\gamma_i B_1^r[\mathcal{I}_x^i\cos(\bar{\omega}_0^r t+\phi_r) + \mathcal{I}_y^i\sin(-\bar{\omega}_0^r t+\phi_r)]. \tag{6}$$

In the reference frame described by the unitary transformation

$$\mathcal{U} = \exp\left(-it\sum_{r=1}^{N_S}\sum_{i=1}^{n_r}\bar{\omega}_0^r\mathcal{I}_z^{\{ri\}}\right). \tag{7}$$

Equations (4) and (6) transform into the effective Hamiltonians

$$\mathcal{H}_{\mathrm{rf}}^{\mathrm{eff}}(t) = -\hbar\sum_{r,s=1}^{N_S}\sum_{i=1}^{N}\gamma_{\{si\}}B_1^r\{\mathcal{I}_x^{\{si\}}\cos[(\bar{\omega}_0^r-\bar{\omega}_0^s)t+\phi_r] + \mathcal{I}_y^{\{si\}}\sin[(-\bar{\omega}_0^r-\bar{\omega}_0^s)t+\phi_r]\}, \tag{8}$$

$$\mathcal{H}_0^{\text{eff}} = -\hbar \sum_{r=1}^{N_S} \sum_{i=1}^{n_r} (\omega_0^{\{ri\}} - \bar{\omega}_0^r) \mathcal{I}_z^{\{ri\}}, \tag{9}$$

$$\mathcal{H}_{\text{int}}^{\text{eff}} = \mathcal{U} \mathcal{H}_{\text{int}} \mathcal{U}^\dagger. \tag{10}$$

In general, the frequency difference $\bar{\omega}_0^r - \bar{\omega}_0^s$ among different species is much larger than $\gamma_i B_1^r$. Moreover, the interaction couplings ω_{ij} and the differences $\omega_0^{\{ri\}} - \bar{\omega}_0^r$ among equal species can be much lower than the rf field strengths. In summary,

$$|\bar{\omega}_0^r - \bar{\omega}_0^s| \gg |\gamma_i B_1^r| \gg |\omega_0^{\{rk\}} - \bar{\omega}_0^r| \gg |\omega_{pq}|,$$

$\forall r \neq s$, $p \neq q$. The statement $|\omega_0^{\{rk\}} - \bar{\omega}_0^r| \gg |\omega_{pq}|$ is the weak coupling condition that provides the simplified terms $\mathcal{I}_z^i \mathcal{I}_z^j$ in Eq. (1). Therefore, under the above conditions the total effective Hamiltonian during the rf pulses becomes

$$\begin{aligned} \mathcal{H}^{\text{eff}} &\simeq -\hbar \sum_{r=1}^{N_S} \omega_1^r \sum_{i=1}^{n_r} [\mathcal{I}_x^{\{ri\}} \cos(\phi_r) + \mathcal{I}_y^{\{ri\}} \sin(\phi_r)] \\ &= -\hbar \sum_{r,i} \omega_1^r \boldsymbol{\mathcal{I}}^{\{ri\}} \cdot \hat{u}_{\phi_r}, \end{aligned} \tag{11}$$

where $\omega_1^r = \gamma_{ri} B_1^r$, $\hat{u}_{\phi_r} = \cos(\phi_r)\hat{x} + \sin(\phi_r)\hat{y}$, and $\boldsymbol{\mathcal{I}}^{\{ri\}} = \mathcal{I}_x^{\{ri\}}\hat{x} + \mathcal{I}_y^{\{ri\}}\hat{y} + \mathcal{I}_z^{\{ri\}}\hat{z}$. Thus, the propagator that describes the rf pulse action is

$$\mathcal{U}_{\mathcal{R}} = \exp\left(i \sum_{r,i} \theta_r \boldsymbol{\mathcal{I}}^{\{ri\}} \cdot \hat{u}_{\phi_r} \right), \tag{12}$$

where $\theta_r = \omega_1^r \Delta t_r$ is the rotation angle around the $\hat{u}_{\phi_r}$ direction for each subsystem r, and Δt_r is the duration of the corresponding pulse.

B. Analytical description of rotations

To describe the effect of rotations on the density operator we will expand it in the basis of irreducible tensor operators, $T_{l,m}^L$, of the SO(3) rotation group. Such basis can be obtained from the irreducible product of the spin polarization operators $T_{l_i,m_i}(s_i)$.[19] For two nuclei the product is defined as

$$T_{l,m}^L = \sum_{m_1,m_2} C_{l_1,m_1,l_2,m_2}^{l,m} T_{l_1,m_1}(s_1) \otimes T_{l_2,m_2}(s_2). \tag{13}$$

$C_{l_1,m_1,l_2,m_2}^{l,m}$ are the Clebsch-Gordan coefficients. The $T_{l_i,m_i}(s_i)$ are irreducible tensors of rank $l_i = 0, 1, \ldots, 2s_i$ and order $m_i = -l_i, -l_i+1, \ldots, l_i$. They constitute a complete set of $(2s_i+1)^2$ operators, which span the space of each nucleus of spin s_i. For N nuclei the Eq. (13) can be used recursively to generate the $T_{l,m}^L$ set for the total system. Consequently, the $T_{l,m}^L$ tensors have rank $l = 0, 1, \ldots, 2\Sigma_{i=1}^N s_i$ and order $m = -l, -l+1, \ldots, l$. The index L accounts for the quantum numbers $l_1, \ldots, l_N, L_2, \ldots, L_{N-1}$, where $|L_{i-1} - l_i| \leq L_i \leq L_{i-1} + l_i$, with $L_1 = l_1$ and $l = L_N$. These quantum numbers represent the coupling scheme between the angular momentum of different nuclei. For a more complete description see Ref. 20. The sum over m_i is restricted to $\Sigma_{i=1}^N m_i = m$.

Therefore, in the frame described by the transformation (7) we represent the density operator by

$$\rho = \sum_{L,l,m} a_{l,m}^L T_{l,m}^L. \tag{14}$$

The $a_{l,m}^L$ are the expansion's coefficients. When the system is formed by only one nucleus, the $T_{l,m}^L$ reduce to the polarization operators $T_{l,m}(s)$, and we drop the L superscript from Eq. (14).

The orthonormalization relation and the phase convention are, respectively,

$$\text{Tr}\{T_{l,m}^{L\dagger} \cdot T_{l',m'}^{L'}\} = \delta_{L,L'} \delta_{l,l'} \delta_{m,m'}, \tag{15}$$

$$T_{l,m}^{L\dagger} = (-1)^m T_{l,-m}^L. \tag{16}$$

By dropping the superscript L and setting $L = L'$, Eqs. (15) and (16) applies to the $T_{l,m}(s)$ operators too. Their representation in the $\mathcal{I}_z$ eigenstate basis is

$$[T_{l,m}(s)]_{pq} = \sqrt{\frac{2l+1}{2s+1}} C_{s,q,l,m}^{s,p}, \tag{17}$$

where $p, q = s, s-1, \ldots, -s$. With these conditions and the fact that ρ is Hermitian we have

$$a_{l,m}^{L*} = (-1)^m a_{l,-m}^L. \tag{18}$$

Under rotations, the irreducible tensors satisfy the following relation:

$$\mathcal{D}(\alpha,\beta,\gamma) T_{l,m}^L \mathcal{D}^\dagger(\alpha,\beta,\gamma) = \sum_{m'=-l}^{l} D_{m',m}^l(\alpha,\beta,\gamma) T_{l,m'}^L, \tag{19}$$

where $\mathcal{D}(\alpha,\beta,\gamma) = e^{-i\alpha\mathcal{I}_z} e^{-i\beta\mathcal{I}_y} e^{-i\gamma\mathcal{I}_z}$ is the rotation operator as function of the Euler angles. $D_{m',m}^l$ are the Wigner functions defined by

$$\langle l', m' | \mathcal{D} | l, m \rangle = \delta_{l',l} D_{m',m}^l. \tag{20}$$

The $|l,m\rangle$ are eigenstates of the angular momentum operator with quantum number l and projection m. We can factorize the three angular dependences in $D_{m',m}^l$,

$$D_{m',m}^l(\alpha,\beta,\gamma) = e^{-im'\alpha} d_{m',m}^l(\beta) e^{-im\gamma}. \tag{21}$$

Explicit forms for the $d_{m',m}^l(\beta)$ functions can be found in Ref. 19. According to equation (12), the action of the rf pulse corresponds to a rotation of an angle θ around a direction restricted to the xy plane making a ϕ angle with the x axis. Therefore, the Euler angles are interrelated by $\alpha = \phi - \pi/2$, $\beta = -\theta$, and $\gamma = -\alpha$. These replaced in Eq. (21) give

$$D_{m',m}^l = e^{i(m-m')(\phi-\pi/2)} d_{m',m}^l(-\theta). \tag{22}$$

In order to make use of property (19), we will apply a pulse that performs the same rotation for all nuclei such that the propagator (12) reduces to the global rotation operator $\mathcal{U} = \exp(i\theta\mathcal{I}_\phi)$. Therefore, the effect of this reading pulse on the density operator (14) is

$$\begin{aligned} \tilde{\rho} &= \mathcal{U}_R \cdot \rho \cdot \mathcal{U}_R^\dagger = \sum_{L,l,m} a_{l,m}^L e^{i\theta\mathcal{I}_\phi} \cdot T_{l,m}^L \cdot e^{-i\theta I_\phi} \\ &= \sum_{L,l,m} a_{l,m}^L \sum_{m'} e^{i(m-m')(\phi-\pi/2)} d_{m',m}^l(-\theta) T_{l,m'}^L. \end{aligned} \tag{23}$$

The transverse magnetization can be represented by the trace of the product of the density operator with the $\mathcal{I}_+$ operator. During the reading time, the magnetization in the laboratory frame is then given by

$$M(t) = \mathrm{Tr}\{\mathcal{U}_F(t) \cdot \tilde{\rho} \cdot \mathcal{U}_F^{\dagger}(t) \cdot \mathcal{I}_+\} e^{i\alpha}. \tag{24}$$

The operator $\mathcal{U}_F(t) = e^{-it(\mathcal{H}_0+\mathcal{H}_{\mathrm{int}})/\hbar}$ is the propagator for the unperturbed Hamiltonian and α is the receiver phase. Now, assuming that the unperturbed Hamiltonian is diagonal in the basis formed by the $\mathcal{I}_z$ eigenstates $|v_i\rangle$, which is true for the weak coupling condition and for the first order quadrupolar Hamiltonian, we find

$$\begin{aligned}\mathrm{Tr}\{T_{l,m}^L \mathcal{U}_F^{\dagger} \mathcal{I}_+ \mathcal{U}_F\} &= \sum_{i,j} \lambda_i^* \lambda_j [\mathcal{I}_+]_{ij} [T_{l,m}^L]_{ji} \\ &= \delta_{m,-1} \sum_{i,j} \lambda_i^* \lambda_j [\mathcal{I}_+]_{ij} [T_{l,-1}^L]_{ji},\end{aligned} \tag{25}$$

where $\lambda_i = e^{-it\langle v_i|\mathcal{H}_0+\mathcal{H}_{\mathrm{int}}|v_i\rangle/\hbar}$. Equations (23)–(25) result in the magnetization

$$M(t) = \sum_{ij} f_{ij}(t) S_{ij}, \tag{26}$$

$$S_{ij} = \sum_{L,l,m} (a_{l,m}^L)^* e^{i(1-m)(\phi-\pi/2)+i\alpha} d_{1,m}^l(-\theta) [A_l^L]_{ij}. \tag{27}$$

The coefficients $f_{ij} = \lambda_i^* \lambda_j$ are the oscillations in the corresponding transition frequencies, S_{ij} are the respective amplitudes, and $[A_l^L]_{ij} = \langle v_i|\mathcal{I}_+|v_j\rangle\langle v_j|T_{l,1}^L|v_i\rangle$ are the weights of each coefficient. The magnetization (26) gives a spectrum with up to $n_f = d\Sigma_{i=1}^N 2s_i/(2s_i+1)$ lines, where $d = \Pi_{i=1}^N (2s_i+1)$ is the system state space dimension. From the hermiticity of ρ and the fact that the identity coefficient $a_{0,0}^0$ is inaccessible for the NMR experiments, we have $d(d+1)/2-1$ independent coefficients to find. To facilitate the tomography process we will apply a coherence selection scheme.

C. Coherence selection scheme

The coherence selection method[21–25] consists of a spectrum average procedure, which selects a desired order m coherence of the spin system density matrix. In our study the following average will accomplish the selection scheme:

$$\bar{S}_{ij}(m') = \frac{1}{N_p} \sum_{n=0}^{N_p-1} S_{ij}(\phi_n, \alpha_n), \tag{28}$$

where $S_{ij}(\phi_n, \alpha_n)$ is the spectrum amplitude obtained with reading pulse of phase ϕ_n and receiver phase α_n. With $\bar{S}_{ij}(m')$ we will obtain a linear system for the different elements of the selected coherence. Choosing the following values for the arguments in Eq. (28)

$$\begin{aligned}\phi_n &= 2\pi n/N_p + \pi/2, \\ \alpha_n &= 2\pi n(m'-1)/N_p,\end{aligned} \tag{29}$$

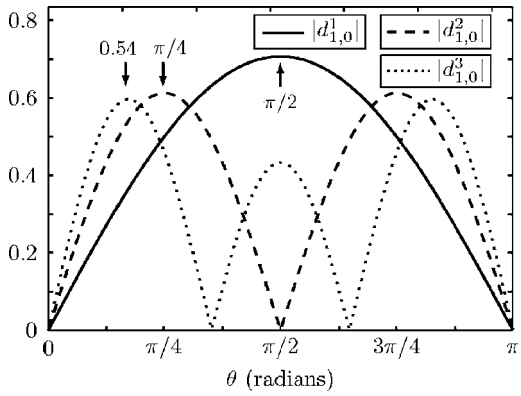

FIG. 1. Angular dependencies of the functions $d_{1,0}^l$ for $1 \leqslant l \leqslant 3$. The arrows indicate the optimum flip angles used to measure the zero order coherences.

$$N_p \geqslant 1 + m' + 2\sum_{i=1}^{N} s_i,$$

and setting the same flip angle θ for all pulses, the summation over n in Eq. (28), after substitution of Eq. (27), transforms into $\Sigma_{n=0}^{N_p-1} e^{i2\pi n(m'-m)/N_p} = N_p \delta_{m,m'}$, which results in

$$\bar{S}_{ij}(m') = \sum_{L,l} (a_{l,m'}^L)^* d_{1,m'}^l(-\theta) [A_l^L]_{ij}. \tag{30}$$

This corresponds to the linear system

$$\begin{aligned}&\boldsymbol{A} \cdot \boldsymbol{x} = \boldsymbol{b}, \\ &[\boldsymbol{A}]_{p(i,j),q(L,l)} = [A_l^L]_{ij}, \\ &[\boldsymbol{x}]_{q(L,l)} = (a_{l,m'}^L)^* d_{1,m'}^l(-\theta), \\ &[\boldsymbol{b}]_{p(i,j)} = \bar{S}_{ij}(m').\end{aligned} \tag{31}$$

For simplicity we will refer to m' just as m. Therefore, for each average we find the set of coefficients $a_{l,m}^L$ for the chosen m, since all the other parameters are known. Only the coefficients with $m \geqslant 0$ must be found, since the negative ones are obtained from the relation (18). In Sec. III A, we show that the linear system (31) is always solvable for the single spin case. For coupled spins systems we limit ourselves to the solution of the specific case of three homonuclear spin 1/2 system in Sec. III B.

One of the advantages of the analytical description given above is the knowledge about the flip angle dependence to each l and m component of the density matrix. Therefore, to improve the sensibility of a given $T_{l,m}^L$ and reduce errors in the rotations of these components, a separated experiment for each rank l can be performed choosing the flip angle θ that maximizes the absolute value of the function $d_{1,m}^l$. As an example, Fig. 1 shows the angular dependencies of the functions $d_{1,0}^l$ for $1 \leqslant l \leqslant 3$.

III. APPLICATIONS

Now, we will apply the general results found in Sec. II to perform the tomography process of some systems of interest.

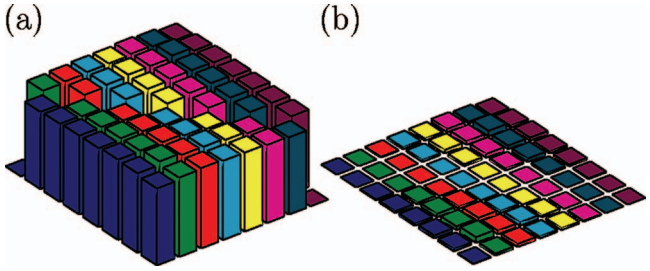

FIG. 2. (Color) (a) Density matrix simulated reconstruction of the superposition $|\Psi\rangle=\frac{1}{2\sqrt{2}}\otimes_{i=1}^{3}(|0\rangle_i+|1\rangle_i)$ implemented by $I=7/2$ nucleus. (b) Absolute deviation of the reconstructed matrix with respect to the expected one.

A. Single spin systems

For a single spin system the spectrum amplitudes are given by the $S_{i,i+1}$ terms in Eq. (26), which depends on the density matrix superdiagonal, $\rho_{i,i+1}$. In fact, for this case, each order m polarization tensor contributes only to the mth density matrix super/subdiagonal, $\rho_{i,i+m}$. Hence, the linear system (31) simplifies to

$$[\boldsymbol{A}]_{i,l}=[A_l]_{i,i+1},$$

$$[\boldsymbol{x}]_l=(a_{l,m})^* d^l_{1,m}(-\theta), \tag{32}$$

$$[\boldsymbol{b}]_i=\bar{S}_{i,i+1}(m),$$

with $1\leqslant i\leqslant 2s$ and $\max(1,m)\leqslant l\leqslant 2s$.

For the single spin system, the irreducible tensors in the A_l coefficients correspond to the polarization tensors $T_{l,1}$. Since these tensors are all linearly independent, each column of the matrix $\boldsymbol{A}$ is linearly independent too. Therefore, with $n_f=2s$ spectral lines we can exactly solve the linear system (30) for $m=0$ and $m=1$, which gives the density matrix diagonal and superdiagonal elements, respectively. Note that there are $2s+1$ diagonal elements. However, since the identity tensor contribution is inaccessible, what can really be measured is the traceless deviation density matrix, $\Delta\rho=\rho-a_{0,0}T_{0,0}(s)$, which is characterized by only $2s$ independent elements. For all the other coherences, $m>1$, the system has more equations than unknowns, resulting in a redundancy that can be solved by a least square method, for example.

It is worthwhile to note that for the spin 3/2 case and for the zero order coherences evaluation, the phase given by relations (29) correspond to the Cyclops average, coinciding for this specific case to the method used in the work of Bonk *et al.*[10]

To illustrate the tomography process for a single spin system we simulate an experiment with a spin 7/2 system under the effect of Zeeman and quadrupolar interactions. The tomography process was used to reconstruct the state $|\Psi\rangle=\frac{1}{2\sqrt{2}}\otimes_{i=1}^{3}(|0\rangle_i+|1\rangle_i)$ that has coherences of all orders. The pulse and receiver phases were used in accordance to Eq. (29). Each coherence selection scheme was repeated with the optimal flip angles to maximize the sensibility to each rank component. In the simulated tomography pulses we applied a deviation of 5% in the flip angles in order to consider calibration errors. Figures 2(a) and 2(b) show, respectively, the reconstructed density matrix and its absolute deviation to the theoretical state. The maximum deviation goes up 7%.

An experimental example of a system that can be treated as a single spin system is the case of a quadrupolar nucleus. A quadrupolar nucleus ($I\geqslant 1/2$), such as ^{7}Li, ^{23}Na, or ^{133}Cs, in a crystalline solid or diluted in a liquid crystalline matrix, produces a macroscopic ensemble that can be well described by a single particle spin Hamiltonian defined solely by the Zeeman and quadrupolar interactions. To illustrate the feasibility of the presented QST method in this system, we follow the main steps of the execution of the Deutsch quantum algorithm in the spin 3/2 ^{23}Na nucleus. This algorithm was executed using the appropriated logical gates implemented by SMP.[18,26] After preparing the initial state $|01\rangle$, step A, the system is put in a complete superposition of states $(|0\rangle+|1\rangle)(|0\rangle-|1\rangle)$ by a Hadamard operation on both qubits (step B). Then, the operations representing constant, $\mathbb{1}$ (identity) and NOT_B, or balanced, CNOT_A and NOT_B-CNOT_A functions are applied (step C). Finally, another Hadamard operation is applied to bring the system to an eigenstate (step D). Whether operations representing constant or balanced functions are applied the final eigenstate is $|01\rangle$ or $|11\rangle$. Figure 3 shows the tomographed density matrices and the corresponding simulations for the intermediate steps obtained during the execution of the Deutsch algorithm. Despite the presence of some unexpected coherences in the final state, the $|01\rangle$ and $|11\rangle$ states are easily recognized. Actually, since the initial states are in very good agreement with the simulations, the presence of the undesirable coherences in the final density matrices are mostly attributed to accumulated errors due to the SMP pulses.

For this experiment, each coherence was selected by the averaged spectrum obtained from nonselective pulses with the phases and receiver angles of Table I, in accordance to Eq. (29). With the purpose to maximize the sensibility to each rank component, each coherence selection experiment was repeated with the flip angles of Table II. The $m=1$ second subcolumn was not used and it is discussed in Sec. III B. It is important to note that the employed pulse widths are of the order of 3 μs, which are much shorter than the 350 μs selective pulses used in the previous work.[10,12]

To verify the quality of the coherence selection process, we performed an experiment following the time evolution of a superposition state implemented on the same ^{23}Na sample used to produce the results of Fig. 3. Figure 4 shows the behavior of each coherence for multiples free evolution times after the preparation of a superposition state. This superposition was prepared with a SMP pulse that had the purpose of creating coherences with almost the same amplitude for all density matrix elements. According to the Hamiltonian (2) the coherences $\rho_{1,2}$ and $\rho_{1,3}$ oscillate with frequency ω_q, while the coherences $\rho_{3,4}$ and $\rho_{2,4}$ oscillate with frequency $-\omega_q$, where the indices 1, 2, 3, and 4 correspond, respectively, to the magnetic quantum numbers 3/2, 1/2, −1/2, and −3/2. This behavior is easily seen in the four graphics from the top of Fig. 4. The absolute values were also plotted, showing approximately a constant value and, therefore, indicating a negligible mixture with other density matrix elements. The remaining coherences, which from

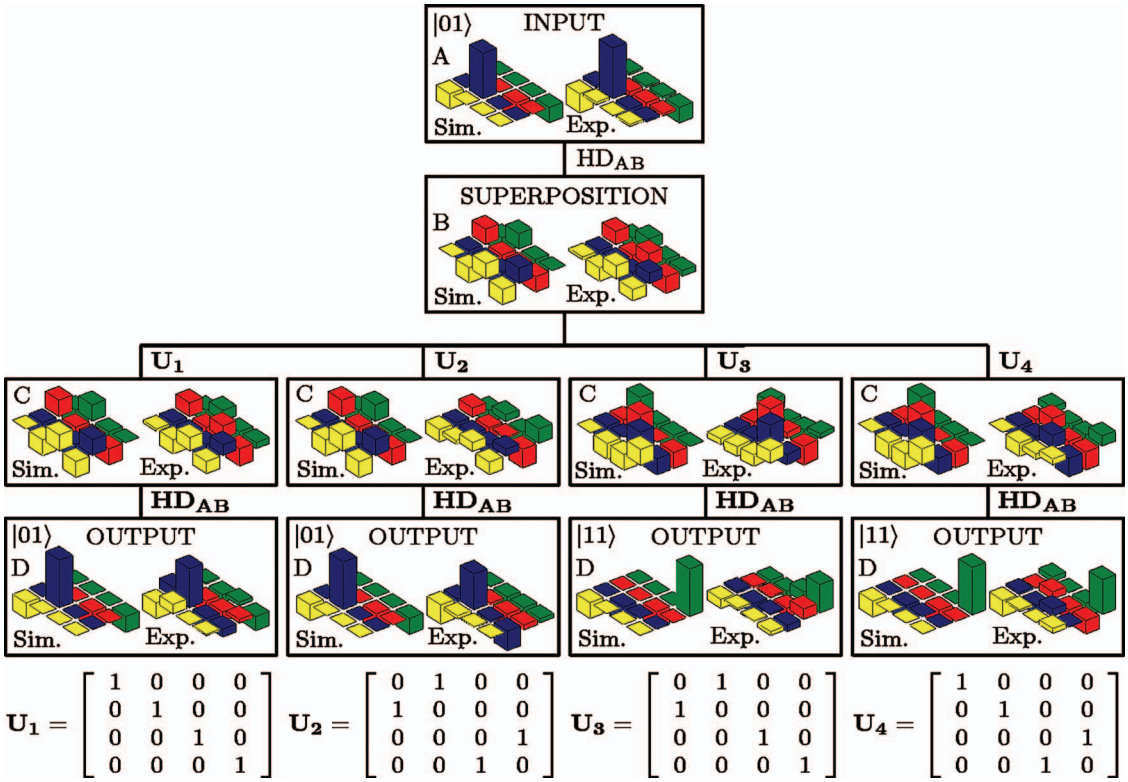

FIG. 3. (Color) Experimentally tomographed density matrices and corresponding simulations for the intermediate steps during the execution of the Deutsch algorithm in the ^{23}Na quadrupolar system. Besides the undesired coherences in the final states, the expected $|01\rangle$ and $|11\rangle$ states are easily recognized. Experimental deviations are mainly attributed to the SMP imperfections.

Eq. (2) should not oscillate, are shown in the bottom of Fig. 4. For the diagonal elements, a time range much greater than one quadrupolar oscillation was taken, evidencing the relaxation effects that bring the density matrix to the equilibrium state proportional to the $\mathcal{I}_z$ operator.

B. Homonuclear coupled spins systems

Contrary to the single spin case, in a coupled spins system the number of spectral lines can be lower than the number of density matrix elements of a selected coherence, making the linear system (31) undetermined. In such cases, it is necessary to select the desired coherence with additional flip angles in order to raise the rank of the linear system (31).

Another problem with coupled spins systems is that there are other combinations of quantum numbers L with the rank $l=0$, besides the identity term. Those components are unobservable for global rotations performed on the system. This can be seen from Eqs. (19) and (25). To solve this problem, we can let the system evolve under the free Hamiltonian before applying the reading pulses. Therefore, those terms with rank $l=0$ evolve to other ranks and make possible their determination. As we are assuming the weak coupling condition, the maximum rank transfer occurs for free evolution delays of $\pi/(\omega_0^i-\omega_0^j)$, for ω_0 in radians.

In order to illustrate the coupled spins system tomography process, we simulate an experiment with three homonuclear coupled spins 1/2. The initial state on which we

TABLE I. Pulse phase ϕ and receiver phase α for the coherence selection experiments for the spin 3/2 case, in radians. Each m column corresponds to an experiment for the mth coherence selection. The flip angles were used in accordance to Table II.

	$m=0$		$m=1$		$m=2$		$m=3$	
n	ϕ	α	ϕ	α	ϕ	α	ϕ	α
0	$\pi/2$	0	$\pi/2$	0	$\pi/2$	0	$\pi/2$	0
1	π	$3\pi/2$	$9\pi/10$	0	$5\pi/6$	$\pi/3$	$11\pi/4$	$2\pi/7$
2	$3\pi/2$	π	$13\pi/10$	0	$7\pi/10$	$2\pi/3$	$15\pi/4$	$4\pi/7$
3	0	$\pi/2$	$17\pi/10$	0	$3\pi/2$	π	$19\pi/4$	$6\pi/7$
4			$21\pi/10$	0	$11\pi/6$	$4\pi/3$	$23\pi/4$	$8\pi/7$
5					$13\pi/6$	$5\pi/3$	$27\pi/4$	$10\pi/7$
6							$31\pi/4$	$12\pi/7$

TABLE II. Flip angles θ, in radians, that maximize the spectrum sensibility to a given component of the density matrix in the irreducible tensor expansion.

l	$m=0$	$m=1$		$m=2$	$m=3$
1	$\pi/2$	0			
2	$\pi/4$	0		$\pi/3$	
3	0.54	0	1.16	0.60	1.23

applied the tomography process is again the superposition $|\Psi\rangle=\frac{1}{2\sqrt{2}}\otimes_{i=1}^{3}(|0\rangle_i+|1\rangle_i)$. We choose typical chemical shift and J couplings values of $\Delta\omega_1=-170$ Hz, $\Delta\omega_2=50$ Hz, $\Delta\omega_3=120$ Hz, $J_{12}=5$ Hz, $J_{13}=8$ Hz, and $J_{23}=3$ Hz, where $\Delta\omega_i=\omega_0^i-\bar{\omega}_0$. The pulse and receiver phases were used in accordance to Eq. (29). Each coherence selection simulation was repeated with the same flip angles shown on Table I with the purpose to maximize the sensibility to each rank component. The second subcolumn of the $m=1$ column contains the secondary maximization angle necessary to raise the linear system's rank. For zero order selection the simulation was repeated for the free evolution times of 7.14, 2.27, and 1.72 ms. These delays maximize the $l=0$ to $l=2$ rank transfer and thus allow the complete determination of all zero order coherences, excluding the identity component. Figure 5(a) shows the reconstructed density matrix. In this simulation we applied again a deviation of 5% in the flip angles in order to consider calibration pulses errors. Figure 5(b) presents the absolute deviation to the expected density matrix. The maximum deviations go up to 3%.

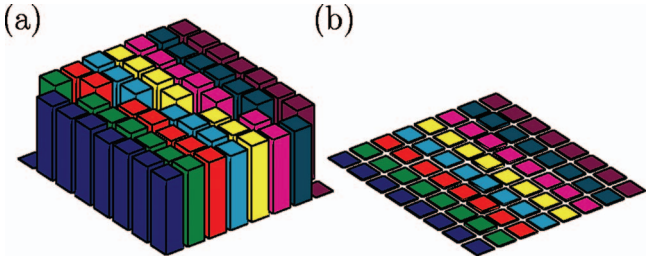

FIG. 5. (Color) Simulation of the tomography process for a three spin 1/2 system. (a) The reconstructed deviation density matrix. (b) The absolute difference to the theoretical matrix.

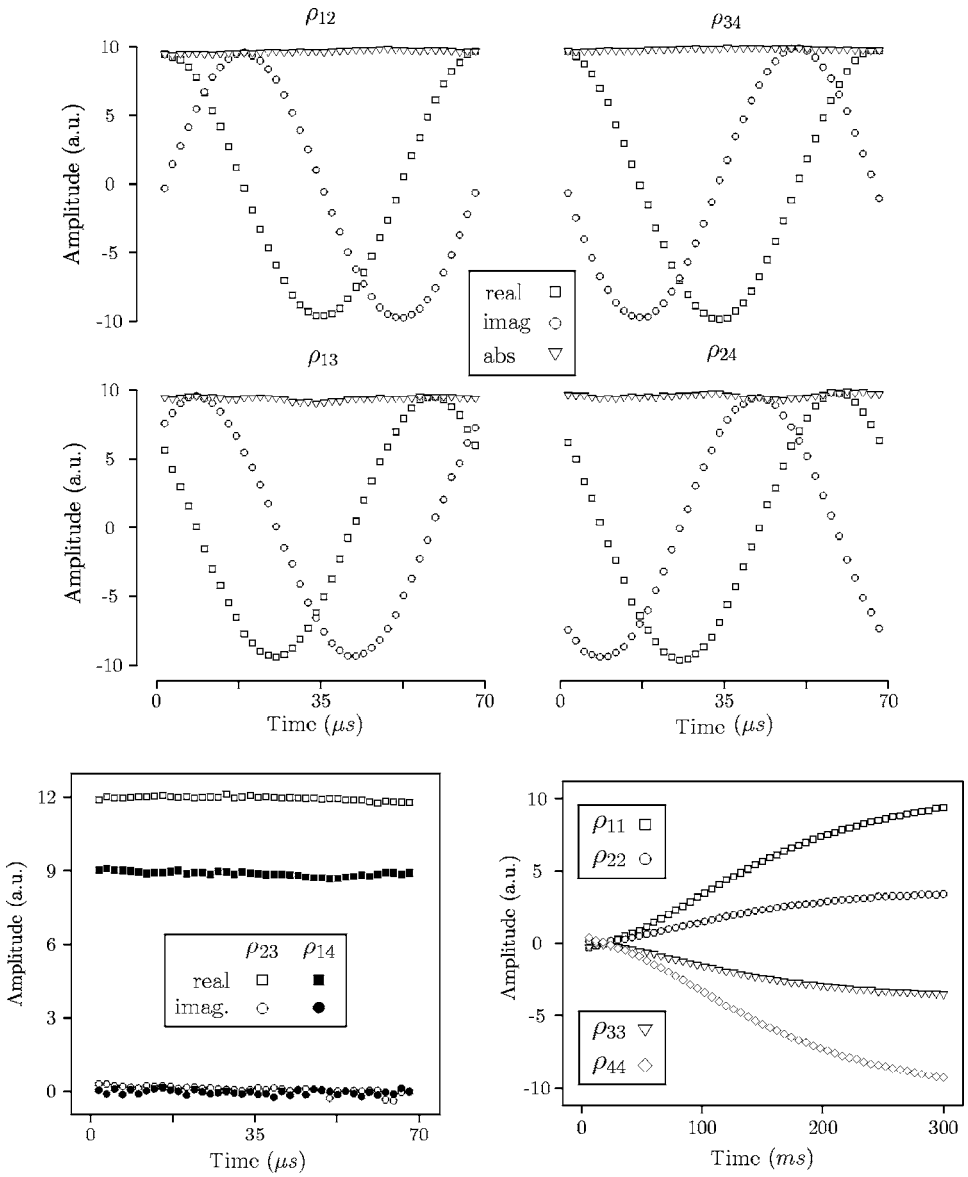

FIG. 4. Experimental density matrix tomography of the free evolution time of an arbitrary superposition state implemented in the ^{23}Na quadrupolar system. The four graphics in the top show the quadrupolar oscillations expected for this system, while the remaining coherences in the bottom stay constant, besides the relaxation effect on the diagonal elements due to the much longer sampling time.

C. Heteronuclear coupled spins systems

For a heteronuclear system the same method can be applied. The system global rotations are accomplished by applying the same flip angle, pulse phase, and receptor phase in the different channels corresponding to the different species. However, it can be necessary to set a receiver frequency offset, $\bar{\omega}_0^r + \Delta\omega_r$, for each r channel in order to simulate the chemical shift evolution in the multiple reference frame (7). This procedure is needed just for zero order coherence determination as discussed in Sec. III B.

A method that utilizes simultaneously different rotations for different species can also be devised. Since in such systems short pulses can easily perform local rotations, the tomography process can be optimized. In fact, a method restricted to coupled single spin 1/2 nucleus already exists[7,8] and it is well established.

IV. EXPERIMENT

The experimental demonstrations of the developed QST method were carried out on ^{23}Na nuclei dissolved in a lyotropic liquid crystal prepared with 20.9 wt % of sodium dodecyl sulfate (95% of purity), 3.7 wt % of decanol, and 75.4 wt % deuterium oxide, following the procedure described elsewhere.[27] The ^{23}Na NMR experiments were performed using a 9.4 T-Varian Inova spectrometer using a 7 mm solid-state NMR probe head. A small sample volume occupying 1/3 of the uniform B_1 field region of the rf coil was used. Pseudopure states and the logical operations used in the Deutsch algorithm were carried out using strongly modulated rf pulses.[18] The lengths of the hard pulses used for QST were smaller than 3 μs. Experiments were performed with a recycle delay of 200 ms.

V. CONCLUDING REMARKS

In this article, we describe a method for NMR quantum state tomography using a coherence selection scheme based on global rotations of the spin system. For a N qubit system implemented by a single quadrupolar nucleus ($I \geqslant 1/2$), the method has the advantage of using only nonselective short pulses, which minimize the relaxation effects and pulse imperfections. Moreover, the effect of short nonselective pulses can be well approximated by ideal rotations, providing a general theoretical description that can be used for any spin quantum number. The method is also advantageous for N coupled homonuclear spins, where previous reported QST methods requires the use of selective pulses. In this case, a drawback is the need of a free evolution period for discriminating the density matrix rank zero components. A direct consequence of the analytical description of the tomography process is the possibility of optimizing the rotations for a particular rank degree. Simulated results show the feasibility of the method for quadrupolar and coupled homonuclear spins. As an experimental demonstration, the flow of implementation of the Deutsch algorithm on a 2-qubit quadrupolar spin 3/2 system was monitored.

ACKNOWLEDGMENTS

The Brazilian Science Foundations FAPESP, CNPq, CAPES, and FINEP supported this work. One of the authors (J.T.) acknowledges Professor P. J. Grandinetti for discussions and suggestions.

[1] U. Leonhardt, H. Paul, and G. M. Dariano, Phys. Rev. A **52**, 4899 (1995).
[2] U. Leonhardt, Phys. Rev. Lett. **76**, 4293 (1996).
[3] R. Walser, J. I. Cirac, and P. Zoller, Phys. Rev. Lett. **77**, 2658 (1996).
[4] A. S. Parkins, P. Marte, P. Zoller, O. Carnal, and H. J. Kimble, Phys. Rev. A **51**, 1578 (1995).
[5] J. P. Amiet and S. Weigert, J. Phys. A **32**, L269 (1999).
[6] R. R. Ernst and G. Bodenhausen, *Principles of Nuclear Magnetic Resonance in One and Two Dimensions* (Clarendon, Oxford, 1987).
[7] I. L. Chuang, N. Gershenfeld, M. G. Kubinec, and D. W. Leung, Proc. R. Soc. London, Ser. A **454**, 447 (1998).
[8] G. L. Long, H. Y. Yan, and Y. Sun, J. Opt. B: Quantum Semiclassical Opt. **3**, 376 (2001).
[9] I. L. Chuang, N. Gershenfeld, and M. Kubinec, Phys. Rev. Lett. **80**, 3408 (1998).
[10] F. A. Bonk, E. R. deAzevedo, R. S. Sarthour, J. D. Bulnes, J. C. C. Freitas, A. P. Guimaraes, I. S. Oliveira, and T. J. Bonagamba, J. Magn. Reson. **175**, 226 (2005).
[11] H. Kampermann and W. Veeman, Quantum Inf. Process. **1**, 327 (2002).
[12] F. A. Bonk *et al.*, Phys. Rev. A **69**, 042322 (2004).
[13] A. K. Khitrin and B. M. Fung, J. Chem. Phys. **112**, 6963 (2000).
[14] R. Das, T. S. Mahesh, and A. Kumar, Phys. Rev. A **67**, 062304 (2003).
[15] G. Yusa, K. Muraki, K. Takashina, K. Hashimoto, and Y. Hirayama, Nature (London) **434**, 1001 (2005).
[16] R. Tycko, Nature (London) **434**, 966 (2005).
[17] Y. Hirayama, A. Miranowicz, T. Ota, G. Yusa, K. Muraki, S. K. Ozdemir, and N. Imoto, J. Phys.: Condens. Matter **18**, S885 (2006).
[18] E. M. Fortunato, M. A. Pravia, N. Boulant, G. Teklemariam, T. F. Havel, and D. G. Cory, J. Chem. Phys. **116**, 7599 (2002).
[19] D. Varshalovich, A. Moskalev, and V. Khersonskii, *Quantum Theory of Angular Momentum* (World Scientific, Singapore, 1988).
[20] B. C. Sanctuary, J. Chem. Phys. **64**, 4352 (1976).
[21] A. Wokaun and R. R. Ernst, Chem. Phys. Lett. **52**, 407 (1977).
[22] G. Bodenhausen, H. Kogler, and R. R. Ernst, J. Magn. Reson. **58**, 370 (1984).
[23] A. D. Bain, J. Magn. Reson. **56**, 418 (1984).
[24] D. Suter and J. G. Pearson, Chem. Phys. Lett. **144**, 328 (1988).
[25] P. J. Grandinetti, Solid State Nucl. Magn. Reson. **23**, 1 (2003).
[26] H. Kampermann and W. S. Veeman, J. Chem. Phys. **122**, 214108 (2005).
[27] K. Radley, L. W. Reeves, and A. S. Tracey, J. Phys. Chem. **80**, 174 (1976).